Calibration methods for laser ablation Rb–Sr geochronology: comparisons and recommendation based on NIST glass and natural reference materials

Stijn Glorie[1*], Sarah E. Gilbert[2], Martin Hand[1], Jarred C. Lloyd[1]

[1] Department of Earth Sciences, University of Adelaide, SA 5005, Australia.

[2] Adelaide Microscopy, University of Adelaide, SA 5005, Australia.

Correspondence to: Stijn Glorie (stijn.glorie@adelaide.edu.au)

Abstract

In-situ Rb–Sr geochronology using LA-ICP-MS/MS technology allows rapid dating of K-rich minerals such as micas (e.g. biotite, muscovite, phlogopite) and K-feldspar. While many studies have demonstrated the ability of the method, analytical protocols vary significantly and to date no studies have provided an in-depth comparison and synthesis in terms of precision and accuracy. Here we compare four calibration protocols based on commonly used reference materials for Rb–Sr dating. We demonstrate that downhole fractionation trends (DHF) for natural biotite, K-feldspar and phlogopite contrast with that for the commonly used Mica-Mg nano-powder reference material. Consequently, Rb–Sr dates calibrated to Mica-Mg can be up to 5% inaccurate and the degree of inaccuracy appears to be unsystematic between analytical sessions. Calibrating to Mica-Mg also introduces excess uncertainty that can be avoided with a more consistent primary calibration material. We propose a calibration approach involving (1) NIST-610 glass as the

primary reference material (PRM) ==for normalization and drift correction== and (2) a natural mineral with similar DHF characteristics to the analysed samples ==as matrix correction RM (MCRM) to correct the Rb/Sr ratio for matrix-induced offsets==. In this work, MDC phlogopite (the source mineral for Mica-Mg nano-powder) was used as the ==MCRM==, consistently producing accurate Rb–Sr dates for a series of natural biotites and K-feldspars with well-characterized expected ages. However, biotite from the Banalasta Adamellite, Taratap Granodiorite and Entire Creek pegmatite are also suitable RMs for Rb/Sr ratio calibration purposes with consistently <1.5% fully propagated uncertainties in our methodological approach. Until calibration using isochronous natural standards as the primary RM becomes possible in data-reduction software, the two-step calibration approach described here is recommended.

Keywords: reaction-cell ICP-MS; in-situ geochronology; Rb–Sr reference materials; calibration standards

1. Introduction

Rubidium-Strontium (Rb–Sr) geochronology using laser ablation – inductively coupled plasma – tandem mass spectrometry (LA-ICP-MS/MS) has become a popular method to constrain the formation or cooling age of potassium-bearing minerals (Gorojovsky and Alard, 2020; Hogmalm et al., 2017; Jegal et al., 2022; Kirkland et al., 2023; Larson et al., 2023; Laureijs et al., 2021; Li et al., 2020; Liebmann et al., 2022; Olierook et al., 2020; Redaa et al., 2021; Rosel and Zack, 2022; Sengun et al., 2019; Tillberg et al., 2021; Tillberg et al., 2020; Wang et al., 2022; Zack and Hogmalm, 2016). In contrast to traditional Rb–Sr dating involving column-chemistry in

44 specialized laboratories, the laser-ablation method allows rapid acquisition of Rb–Sr dates directly

45 from thin sections or rock blocks with minimal sample preparation. The method involves the use

46 of an ICP-MS/MS, equipped with a reaction cell where isobaric isotopes can be chemically

47 separated due to their significant differences in reactivity with an introduced reaction gas (Balcaen

48 et al., 2015 and references therein). Applied to Rb–Sr geochronology, CH_3F, SF_6, O_2 and N_2O

49 have been used as reaction gasses (e.g. Hogmalm et al., 2017; Moens et al., 2001; Zack and

50 Hogmalm, 2016), with the latter being the most widely used for quadrupole ICP-MS/MS due to

51 its high reactivity. However, published analytical methodologies for LA-ICP-MS/MS Rb–Sr

52 dating vary significantly beyond the applied reaction gas (Table 1). Reported laser conditions

53 (fluence and repetition rate) are largely laser-wavelength dependent with common conditions

54 being either ~5 - 7 $J.cm^{-2}$ / 10 Hz for 213nm lasers, especially during initial development work

55 (e.g. Hogmalm et al., 2017; Laureijs et al., 2021; Rosel and Zack, 2022; Sengun et al., 2019;

56 Tillberg et al., 2020; Zack and Hogmalm, 2016) or ~2 - 4 $J.cm^{-2}$ / 5 Hz for 193nm lasers (e.g.

57 Kirkland et al., 2023; Larson et al., 2023; Li et al., 2020; Liebmann et al., 2022; Olierook et al.,

58 2020; Redaa et al., 2021). The applied calibration protocols for mass discrimination and elemental

59 fractionation, however, vary more significantly.

60 We define three types of reference materials (RM) in this manuscript:

61   (1) The Primary RM (PRM) has a homogenous isotopic composition and is used for

62   normalisation and drift correction;

63   (2) The matrix correction RM (MCRM) has a heterogenous isotopic composition but well-

64   known age and is used to correct the Rb/Sr ratio for systematic matrix-induced off-sets

65   between the PRM and mineral samples.

66 (3) The secondary RM (SRM) has a well-known age and a similar composition to the analysed

67 samples and is used to verify the accuracy of the calibration protocol.

68 Most published work uses a glass reference material as PRM, with NIST-610 being most popular

69 to correct for drift and calibrate the Sr isotopic ratios. Rb/Sr ratios are most commonly calibrated

70 against Mica-Mg, a phlogopite prepared as a pressed nano-powder pellet, regardless of the

71 analysed mineral (micas in most published work). However, the approach varies, with some

72 methods directly calibrating to Mica-Mg as the PRM (e.g. Gorojovsky and Alard, 2020; Hogmalm

73 et al., 2017; Li et al., 2020; Redaa et al., 2021; Rosel and Zack, 2022; Sengun et al., 2019; Wang

74 et al., 2022) and others using NIST-610 as the PRM followed by a correction for matrix-dependent

75 fractionation against Mica-Mg as MCRM (e.g. Liebmann et al., 2022; Olierook et al., 2020).

76 Secondary RMs, used to verify the accuracy of obtained dates, are either glass reference materials

77 (e.g. Larson et al., 2023; Laureijs et al., 2021; Rosel and Zack, 2022) or in-house natural materials

78 such as the La Posta biotite (Zack and Hogmalm, 2016), the MDC phlogopite (Redaa et al., 2021),

79 or the CK001 biotite (Olierook et al., 2020).

80 In addition, laser-induced down-hole fractionation (DHF) can occur during ablation and aerosol

81 condensation processes and is most apparent when ratioing elements with contrasting volatilities

82 (e.g. Jackson and Günther, 2003; Košler et al., 2005; Longerich et al., 1996). Elemental Sr is more

83 refractory than the volatile Rb and hence has a high potential to fractionate during laser ablation

84 (Zack and Hogmalm, 2016). A small number of studies have directly compared different

85 calibration approaches and have described differences in Rb–Sr DHF behaviour between

86 commonly used reference materials (e.g. Redaa et al., 2021; Wang et al., 2022). However,

87 systematic comparisons between data reduction protocols, tested with natural materials, are limited

88 in the current literature. Here, we compare four different calibration approaches for a series of

89   natural biotite and K-feldspar samples. The samples were taken from quickly cooled igneous rocks,

90   eliminating potential diffusion-related issues when comparing dates of different minerals. Hence,

91   the well-constrained igneous crystallization ages are the expected reference ages for the analysed

92   samples and one of the biotite samples has previously been dated by the Rb–Sr ID-TIMS method.

93   The calibration approaches we compare are:

94   (A) NIST-610 as the PRM for both ^{87}Rb/^{87}Sr and ^{87}Sr/^{86}Sr ratios plus MDC phlogopite as MCRM;

95   (B) NIST-610 as the PRM for both ^{87}Rb/^{87}Sr and ^{87}Sr/^{86}Sr ratios plus Mica-Mg pressed pellet as
96   MCRM;

97   (C) Mica-Mg as the PRM for ^{87}Rb/^{87}Sr ratios and NIST-610 as the PRM for ^{87}Sr/^{86}Sr ratios;

98   (D) Mica-Mg as the PRM for both ^{87}Rb/^{87}Sr and ^{87}Sr/^{86}Sr ratios

99   We discuss the differences between these approaches in terms of accuracy and precision, and

100   highlight the importance of monitoring and correcting down-hole fractionation with appropriate

101   reference materials.

102

2. Sample descriptions

2.1. MDC phlogopite and Mica-Mg nano powder

105   Mica-Mg nano-powder is used as a reference material for Rb–Sr dating. It consists of crushed

106   phlogopite from Bekily (Madagascar) with a high Rb (1300 $\pm$ 40 µg.g^{-1}) and low Sr (27 $\pm$ 3 µg.g^{-}

107   ^{1}) concentration (Redaa et al., 2023 and references therein). MDC is natural phlogopite, which was

108   sourced from the same locality as Mica-Mg (Redaa et al., 2021). The reference age for both

109   materials is 519.4 $\pm$ 6.5 Ma and the initial ^{87}Sr/^{86}Sr ratio is 0.72607 $\pm$ 0.0007 (2SE uncertainties),

110 constrained from a diopside (low-Rb mineral) that occurs in the same location (Hogmalm et al.,

111 2017). However, for Mica-Mg some pellet to pellet variation in both Rb/Sr and Sr/Sr ratios has

112 been observed (Jegal et al., 2022; Redaa et al., 2023).

113 **2.2. Entire Creek pegmatite**

114 The Entire Creek sample was taken from a deformed pegmatite in the Harts Range meta-igneous

115 complex of central Australia, in the same location as described by Mortimer et al. (1987). The

116 pegmatite cross-cuts folded and foliated amphibolites, is composed of coarse-grained quartz,

117 plagioclase, alkali feldspar and biotite, with the latter defining a strong axial-plane foliation to

118 folds outlined by the pegmatite. Biotite and whole-rock Rb/Sr and Sr/Sr isotope ratios, obtained

119 by ID-TIMS at the University of Adelaide, are reported in Mortimer et al. (1987) and define a 7-

120 point (3 biotite and 4 whole rock analyses) isochron age of $312.1 \pm 1.8 / 5.1$ Ma (95% confidence

121 uncertainties, without / with overdispersion), recalculated in IsoplotR (Vermeesch, 2018), using

122 the Villa et al. (2015) Rb–Sr decay constant of $1.3972 \pm 0.0045 \times 10^{-11}$ a^{-1} (Appendix 1).

123 **2.3. Banalasta Adamellite (Bundarra Suite)**

124 The S-type Banalasta Adamellite forms the southern end the Bundarra Batholith in the Southern

125 New England Orogen in eastern Australia (e.g. Flood and Shaw, 1975; Jeon et al., 2012;

126 Rosenbaum et al., 2012; Shaw and Flood, 1981). The Bundarra Batholith is an elongate north-

127 south trending magmatic suite, spanning approximately 200 km. The Banalasta Adamellite is

128 approximately 40 km in diameter and has sharp contacts with surrounding metasediments with a

129 contact metamorphic aureole characterised by fine-grained cordierite-bearing assemblage at the

130 pluton margin grading out to regional prehnite-pumpellyite metagreywacke assemblages over a

131 distance of approximately 3 km (Flood and Shaw, 1977). Internally the granite is massive, coarse-

132 grained granitoid containing approximately equal proportions of K-feldspar and plagioclase,

133 together with accessory apatite, zircon and monazite. Biotite predominantly occurs in multi-grain

134 clots together with quartz, plagioclase, magnetite, zircon and apatite. In rare cases they contain

135 relic garnet, suggesting they formed from hydration of garnet entrained from the granitic source

136 region.

137 Melt-precipitated zircon from the Banalasta Adamellite gives zircon U-Pb ages of 286.2 ± 2.2 Ma

138 (Black, 2007), 289.2 ± 1.7 Ma (Jeon et al., 2012) and 282 ± 4 Ma (Phillips et al., 2011). Whole

139 rock Rb–Sr data from the Bundarra Suite gives an age of 285 ± 15 Ma (n = 6/7, MSWD = 0.4).

140 When additional feldspar Rb–Sr data are included in the isochron, the isochron age is 283 ± 10 Ma

141 (n = 9/10, MSWD = 0.24) (Appendix 2). Both isochron dates were recalculated using the data from

142 Flood and Shaw (1977) and the decay constant from Villa et al. (2015). Additionally, Hensel et al

143 (1995) reported a model whole rock Rb–Sr age of 287 ± 10 Ma for a group of 16 samples from the

144 Bundarra Suite. Overall, it is evident that Rb–Sr age data is similar to the ages of melt precipitated

145 zircon, consistent with the lack of evidence for extended fractional crystallisation (Jeon et al 2012).

146 The samples used in this study come from the same location as Black (2007) that has a granitic

147 zircon of 286.2 ± 2.2 Ma, as well as a second location approximately 800 meters away.

148

2.4. Taratap Granodiorite

150 The Taratap Granodiorite in the Delamerian Orogenic belt in southern Australia is classified as S-

151 type, calc-alkaline with a composition dominated by microcline megacrysts (c. 3–4 cm in length),

152 which define a NNE-trending magmatic fabric in a coarse-grained groundmass of plagioclase,

153 quartz, K-feldspar and biotite, with accessory zircon, apatite, and monazite. Low-temperature

154 alteration is evident in thin section by the presence of chlorite–muscovite–titanite and minor

155 allanite (Burtt and Abbot, 1998). The sample was chosen for analysis because the timing of

156 emplacement is tightly constrained by a zircon U-Pb ID-TIMS age of 497.11 ± 0.56 Ma (^{206}Pb/^{238}U

157 weighted mean age, 95% confidence interval uncertainty, MSWD = 1.8, n = 6) and an apatite Lu-

158 Hf age of 497.1 ± 5.5 Ma (MSWD = 1.1, n = 38) (Glorie et al., 2023 and references therein).

159

160 ### 3. Analytical methods

161 All Rb–Sr analyses were conducted at Adelaide Microscopy, University of Adelaide, using an

162 Agilent 8900x ICP-MS/MS, coupled to a RESOlution-LR ArF excimer (193 nm) laser ablation

163 system. A squid mixing device (Laurin Technic) was used to smooth the pulsed laser signal

164 between the laser and the mass-spectrometer. The instrument parameters follow those reported in

165 Redaa et al. (2021), with ablation in a He atmosphere (350 mL.min^{-1}), mixed with Ar (890 mL.min^{-}

166 ^{1}) as the carrier gas and N_2 (3.5 mL.min^{-1}) added before the ICP torch to enhance the signal

167 sensitivity. N_2O (0.37 mL.min^{-1}) was used as the reaction gas to separate ^{87}Sr from ^{87}Rb. The ^{86}Sr

168 and ^{87}Sr isotopes were measured as their oxide reaction products (e.g. ^{87}Sr^{16}O) with a mass shift

169 of 16 amu between the two quadrupole mass analysers (e.g. Q1 = 87 m/z, Q2 = 103 m/z). Despite

170 the high reaction efficiency of ^{87}Sr, residual unreacted Sr prevents direct measurement of ^{87}Rb.

171 Instead, ^{85}Rb was measured as a proxy for ^{87}Rb and calculated assuming natural isotopic

172 abundance. The samples and reference materials were ablated using a circular laser beam of 67

173 μm diameter, a fluence of 3.5 J.cm^{-2}, and repetition rate of 5 Hz. Further details are presented in

174 Table 2. A total of three analytical sessions were conducted, with largely identical instrumental

175 parameters between the different sessions. The ICP-MS was tuned to a sensitivity which kept Rb

176 in pulse mode in Mica-Mg (the material with the highest Rb concentration), negating the

177 requirement for additional pulse-analogue (P/A) corrections.

178 For each analytical session, NIST-610, Mica-Mg and MDC were used as reference materials for

179 calibration purposes. All data was processed in LADR (Norris and Danyushevsky, 2018) using an

180 in-built data reduction algorithm that calculates error correlations (Pearson correlation coefficient)

181 from the raw isotopic ratios for each sweep in an analysis, in the same way as for U-Pb data

182 reduction. Isotope ratios were calculated by: (1) background subtraction, (2) correcting down-hole

183 fractionation (DHF) against the PRM, (3) averaging the DHF corrected ratios of each sweep in the

184 analysis, and then (4) normalising to the PRM to correct for matrix independent instrument mass

185 bias and drift. LADR applies a robust uncertainty propagation using the total uncertainty budget

186 of the measured quantified ratios. An example of an `uncertainty tree`, which can be queried for

187 every analysis, is given in Appendix 3. The reader is referred to the LADR software manual

188 (https://norsci.com/?p=ladr-support) for further details.

189 Normalisation of the measured Rb/Sr and Sr/Sr ratios was conducted with two different reference

190 materials (NIST-610 and Mica-Mg), following the four analytical protocols outlined above (A-D).

191 The reference $^{87}Rb/^{87}Sr$ and $^{86}Sr/^{87}Sr$ ratios used for Mica-Mg were 83.4 ± 1.0 and 0.53981 ±

192 0.00070, respectively (Hogmalm et al., 2017). For NIST-610, the $^{87}Rb/^{87}Sr$ was calculated from

193 ppm data (GeoREM preferred values) as 3.28 ± 0.03 and for the $^{86}Sr/^{87}Sr$ ratio, the reference value

194 of 1.409048 ± 0.000036 was used (Woodhead and Hergt, 2001). For each normalization protocol,

195 DHF corrections of the $^{87}Rb/^{87}Sr$ ratios were applied based on the DHF behaviour of the applied

196 PRM. No DHF correction was applied to the $^{86}Sr/^{87}Sr$ ratios. Where NIST-610 was used as the

197 PRM, MDC phlogopite or Mica-Mg were used as MCRM to correct the $^{87}Rb/^{87}Sr$ ratios for matrix-

198   dependant fractionation (cfr. Roberts et al., 2017 for U/Pb ratios; Simpson et al., 2022 for Lu/Hf

199   ratios).

200   All mica samples (including biotite samples and MDC phlogopite) were ablated with the laser

201   ablating parallel to cleavage. The Bundarra and Taratap samples were analysed in thin section and

202   optical microscopy (birefringence) was used to only select ablation targets with upright (± 10°)

203   cleavage. The coarse Entire Creek biotites were mounted as mica-books using a vice to prevent

204   air-gaps between individual mica sheets, with the 'pages' of the book mounted upright exposing

205   multiple cleavage planes perpendicular to the surface.

206   For each sample and reference material, inverse isochron Rb–Sr dates (Li and Vermeesch, 2021)

207   were calculated in IsoplotR (Vermeesch, 2018), based on the processed ^{87}Rb/^{87}Sr and ^{86}Sr/^{87}Sr

208   ratios, their 2SE uncertainties, and the calculated error correlations. Reported inverse isochron

209   uncertainties are fully propagated 95% confidence intervals, including the uncertainty on the decay

210   constant and added uncertainty for overdispersion where required (calculated in IsoplotR). The

211   exceptions are the inverse isochron dates for MDC and Mica-Mg when used as MCRMs, which

212   are used to correct the Rb/Sr ratios after calibrating to NIST-610. For these cases the reported

213   uncertainties are 95% confidence uncertainties without external uncertainties (as the external

214   uncertainties would otherwise be applied twice to the isochron dates of the analysed samples).

215   Session-dependant correction factors (CF) were calculated from the measured ^{87}Rb/^{87}Sr ratio for

216   MDC and Mica-Mg (after drift corrections) and compared to the reference value (calculated from

217   the published age for both MDC and Mica-Mg of 519.4 ± 6.5 Ma; Hogmalm et al., 2017; Redaa

218   et al., 2021). These CF values (= measured ratio/expected ratio) were subsequently applied to each

219   unknown analysis when calibrated to either MDC or Mica-Mg. Finally, the uncertainties on the

220   MDC and Mica-Mg dates are propagated to the reported Rb–Sr isochron uncertainties for each

221   NIST-610 calibrated sample using the quadratic addition of the relative uncertainties.

222

223   **4. Results**

224   **4.1. Downhole fractionation trends**

225   In this section, we compare the downhole fractionation (DHF) trend of the ^{87}Rb/^{87}Sr ratio between

226   the analysed feldspars and micas and the reference materials (NIST-610 and Mica-Mg) (Fig. 1).

227   The obtained fractionation trends do not vary significantly between different sessions; however,

228   data from analytical session 3 is presented as it contains data for all analysed samples presented in

229   this paper. The DHF trends were calculated in LADR and individual scatter plots can be found in

230   Appendix 4. As shown, The DHF trends for the analysed biotite, phlogopite and K-feldspar

231   samples are internally consistent, showing ~10% increase in Rb/Sr ratio over the first 20 s of

232   ablation, followed by a flatter trend in the subsequent 20 s. NIST-610 shows a similar trend of

233   increasing Rb/Sr ratio with ablation time, however the amplitude of the DHF curve is more

234   subdued compared to the natural samples (~3.5% increase in the first 20 s ablation). In contrast,

235   the DHF pattern for Mica-Mg shows an oscillating trend, increasing for the first ~10 s of ablation

236   and then dropping for the subsequent ~30 s of ablation (Fig. 1).

237

238   **4.2**. **Within-session reproducibility of ^{87}Rb/^{87}Sr and ^{86}Sr/^{87}Sr ratios**

239   Figure 2 shows the within-session variability (prior to drift correction) of the ^{87}Rb/^{87}Sr and

240   ^{86}Sr/^{87}Sr ratios for both PRMs NIST-610 and Mica-Mg in analytical session 3. The reference

241   materials are considered homogenous in both isotopic ratios, meaning that any variations are

242   purely due to differences in the ablation characteristics from spot to spot. As shown, the measured

243   ^{87}Rb/^{87}Sr ratios and ^{86}Sr/^{87}Sr ratios are significantly more consistent for NIST-610 compared to

244   Mica-Mg (both measured using the same analytical conditions and spot size). The maximum

245   within-session variability (=min-max range) in the ^{87}Rb/^{87}Sr ratio is < 3% for NIST-610, compared

246   to > 8% for Mica-Mg. The ^{86}Sr/^{87}Sr ratio is more consistent for both RMs, however, the uncertainty

247   on individual analyses is approximately 3× larger for Mica-Mg compared to NIST-610. ICP-MS

248   mass-bias drift is minimal for both isotope ratios in NIST-610, with only a slight increase in the

249   Rb/Sr ratio over the first 2-3 hours of analysis. As both Mica-Mg and NIST-610 were analysed

250   sequentially in the same analytical session, the apparent 'drift' in the Mica-Mg ^{86}Sr/^{87}Sr ratios are

251   due to variations in ablation rather than changes in the ICP-MS mass bias.

252   **4.3. Isochron Rb–Sr dates for natural K-feldspars and micas**

253   Inverse isochron plots and resulting Rb–Sr dates are presented for each analytical protocol in

254   Appendix 5. Summary plots are shown in Figure 3. The data-table with the input ^{87}Rb/^{87}Sr and

255   ^{86}Sr/^{87}Sr ratios is accessible from Figshare via the link in the data availability section. For the

256   Bundarra samples, the biotite isochrons are anchored to apatite Rb/Sr ratios, given that the apatites

257   commonly occur as inclusions within biotite. For the K-feldspars, the isochrons are anchored to

258   plagioclase, given that the analysed K-feldspars often show minor exsolution with plagioclase.

259   However, the choice of anchoring mineral gives no difference in the obtained biotite and K-

260   feldspar inverse isochron Rb/Sr dates. For the Taratap sample, isochron anchoring was conducted

261   to a combination of plagioclase and apatite in session 1, but only plagioclase in sessions 2 and 3,

262   given the limited occurrence of apatite in thin section. For the Entire Creek biotite sample,

263   anchoring was conducted to whole-rock ^{86}Sr/^{87}Sr ratios from Mortimer et al. (1987). The MDC

264 and Mica-Mg isochrons were anchored to an initial $^{86}Sr/^{87}Sr$ ratio of 1.3773 ± 0.0013 and

265 calibrated to the published age of 519.4 ± 6.5 Ma (Hogmalm et al., 2017; Redaa et al., 2021).

266 The summary of obtained inverse Rb–Sr dates is presented in Table 3. As shown, there is only

267 marginal variation in the absolute biotite dates between the three analytical protocols involving

268 Mica-Mg, either as the PRM for Rb/Sr ratios (protocols C & D) or as a MCRM (protocol B).

269 Hence, in order to evaluate the accuracy of the obtained Rb–Sr dates against the expected

270 references ages for each sample, we only compare the first two analytical protocols (NIST-610 as

271 the PRM and either: (A) MDC or (B) Mica-Mg as MCRM).

272 Figure 4 compares the obtained Rb–Sr inverse isochron dates to the expected ages for the three

273 samples, that were analysed over two or three analytical sessions. The uncertainties for the K-

274 feldspar dates are not shown as they are too large to be useful (due to the relatively low radiogenic

275 nature of typical K-feldspar versus micas), here we only compare the accuracy of the absolute

276 dates. As shown, analytical protocol (A) involving NIST-610 as PRM and MDC phlogopite as

277 MCRM consistently gives the most accurate Rb–Sr dates across all different analytical sessions.

278 For this analytical protocol, the Rb–Sr biotite dates for the Bundarra samples are 287.1 ± 2.4 Ma,

279 284.7 ± 3.0 Ma, 287.7 ± 2.3 Ma and 285.7 ± 2.6 Ma (between two samples over two analytical

280 sessions), which are in excellent agreement with the published zircon U-Pb age of 286.2 ± 2.2 Ma

281 (Black, 2007) from the same outcrop. The K-felspar dates of 290 ± 14 Ma, 285 ± 15 Ma, 290 ± 37

282 Ma and 288 ± 37 Ma are in excellent agreement as well but are less useful to evaluate age

283 accuracies given their larger uncertainties. Similarly for the Taratap sample, the obtained biotite

284 Rb–Sr dates of 499.4 ± 3.6 Ma and 495.7 ± 4.0 Ma as well as the (imprecise) K-feldspar Rb–Sr

285 dates of 500 ± 30 Ma, 501 ± 50 Ma and 495 ± 35 Ma are in excellent agreement with the zircon

286 U-Pb ID-TIMS age of 497.1 ± 0.6 Ma as well as the apatite Lu-Hf age of 497.1 ± 5.5 Ma for the

287   same sample (Glorie et al., 2023). Hence, the combined dataset suggests that the biotite, K-feldspar

288   and zircons record the same (crystallization) age for both the Bundarra and Taratap samples. The

289   Entire Creek biotite gave consistent Rb–Sr dates of 310.7 ± 1.5 Ma and 311.6 ± 3.1 Ma, in excellent

290   agreement with the ID-TIMS age of $312.1 \pm 1.8 / 5.1$ Ma (95% confidence uncertainties, without

291   / with overdispersion), based on the Rb/Sr ratios in Mortimer et al. (1987), recalculated with the

292   Villa et al. (2015) Rb–Sr decay constant.

293   **5. Discussion**

294   **5.1. Downhole fractionation corrections**

295   Few previous studies have reported Rb–Sr DHF trends for a series of artificial reference materials

296   (i.e. glass standards and pressed pellets; Redaa et al., 2021; Wang et al., 2022). However, to the

297   best of our knowledge, DHF trends have not been evaluated for natural materials with the

298   exception of phlogopite MDC (Redaa et al., 2021). In our experiments, DHF is more pronounced

299   in natural micas and K-feldspar than observed for the NIST-610 glass and Mica-Mg pressed pellet,

300   when ablated under the same analytical conditions (Fig. 1). Comparatively, Mica-Mg appears least

301   appropriate to correct the analysed samples for DHF, given its systematically different DHF trend.

302   NIST-610 shows less DHF compared to the analysed micas and K-feldspars but its trend is more

303   systematic (similar shape with lower amplitudes). Thus, correcting for DHF against NIST-610

304   reduces the observed DHF for the analysed samples, while Mica-Mg significantly under-corrects

305   for DHF or accentuates it when applied to minerals. MDC biotite would be the most appropriate

306   choice for DHF correction as it behaves very similar to the analysed mica and K-feldspar samples.

307   However, as with most natural materials, MDC is not sufficiently homogenous in $^{87}Rb/^{87}Sr$ ratio

308   to be used as a PRM. While the shape or slope of DHF trends can vary depending on laser

309   conditions (spot size, frequency and fluence), it cannot be eliminated for elements with contrasting

310 volatilities such as Rb and Sr. However, based on the presented data, the use of NIST-610 is the

311 more appropriate reference material to correct for DHF and Mica-Mg would exacerbate instead of

312 reduce the effects of DHF.

313 If no DHF correction is applied, accurate data can only be achieved if exactly the same signal

314 interval is selected in both the RM and sample. If there is a residual DHF slope on the sample

315 Rb/Sr ratios that is different to the RM (e.g. crystalline material versus Mica-Mg), then selecting

316 a shorter signal interval can significantly bias Rb/Sr ratios and hence the apparent age.

317

318 **5.2. Mica-Mg vs NIST-610 and MDC as calibration standards**

319 **5.2.1. Uncertainty comparisons**

320 The contributions to the propagated uncertainties of individual analyses from the reference

321 materials (average signal precision and calibration curve misfit) are much larger when calibrating

322 to Mica-Mg compared to NIST-610 for both ^{87}Rb/^{87}Sr and ^{86}Sr/^{87}Sr ratios (Fig. 5). For example,

323 in analytical session 1, the obtained uncertainties for individual ^{87}Rb/^{87}Sr ratios for the Entire

324 Creek biotite sample are more than double when using Mica-Mg compared to NIST-610 as the

325 PRM (Fig. 5). As a result, the choice of Mica-Mg instead of NIST-610 as the PRM will increase

326 the uncertainties on each analysis, and might consequently mask the presence of multiple data

327 populations. It will also introduces excessive uncertainties onto the calculated isochron dates.

328 The use of Mica-Mg as calibration standard for ^{86}Sr/^{87}Sr ratios most significantly affects the

329 isochron precision of low-radiogenic samples such as K-feldspar samples. As shown in Table 3

330 and Figure 5, the uncertainty on the K-feldspar isochron dates can be up to 2× larger, compared to

331 other calibration methods. Furthermore, the resulting MSWD values on the isochron regressions

332 are consistently < 0.3 (Table 3), suggesting excessive uncertainties on individual data-points. For

333   the more radiogenic biotite samples, the larger uncertainties in $^{86}Sr/^{87}Sr$ ratios have negligible

334   effects to the precision on the isochron dates.

335   The precision of the calibrated $^{87}Rb/^{87}Sr$ ratios is more important to the isochron uncertainty of

336   highly radiogenic materials, such as most types of micas. Calibrating to NIST-610 versus Mica-

337   Mg yields either more precise biotite isochron dates or identical precision. However, when NIST-

338   610 is used as the PRM, uncertainty propagation from the MCRM (MDC or Mica-Mg) leads to

339   either identical or slightly worse isochron uncertainties compared to using Mica-Mg as PRM (Fig.

340   5; Table 3). The difference relates to the degree of overdispersion. The larger uncertainties on the

341   Rb/Sr ratios when using Mica-Mg as PRM result in lower MSWD values, reducing the uncertainty

342   on the isochron regression. This excess uncertainty when calibrating to Mica-Mg might mask

343   meaningful geological scatter in Rb/Sr ratios and it is, therefore, advisable to produce isochrons

344   based on data with the best possible analytical precision.

345   In summary, Mica-Mg should not be used as calibration standard for $^{86}Sr/^{87}Sr$ ratio calculations

346   for low-radiogenic samples as it introduces excessive uncertainties to age calculations. For high-

347   radiogenic samples, using Mica-Mg as the PRM also introduces larger uncertainties to individual

348   data-points compared to using NIST-610, but there is no significant difference in propagated

349   uncertainty after secondary correction to either MDC or Mica-Mg. For Rb/Sr ratio calibrations,

350   NIST-610 is more consistent, resulting in lower uncertainties on individual Rb/Sr ratios. When

351   there is no overdispersion, this results in better isochron age precision. However, overdispersion

352   can be masked by the increased uncertainties on Rb/Sr ratios, resulting in better apparent precision

353   when data is calibrated to Mica-Mg.

354   **5.2.2. Accuracy comparisons**

355 It has been observed previously that Rb–Sr dates are offset from their expected ages when

356 calibrated to the NIST-610 reference material (e.g. Gorojovsky and Alard, 2020; Wang et al.,

357 2022). In contrast, Mica-Mg seems to better reproduce expected ages, although the significant

358 uncertainties obtained for natural materials in previous studies render appropriate accuracy testing

359 difficult. For example, Wang et al. (2022) compares measured to expected Rb–Sr dates for three

360 samples with known ages. The best achieved uncertainty in their experiment was ~2.6% for one

361 sample, while for the other samples the reported uncertainties are ~5.6 and 6.3 %. Similarly, the

362 accuracy comparisons in Gorojovsky and Alard (2020) use the Monastery phlogopite, with a

363 precision of ~4% when calibrated to Mica-Mg. Both papers report data normalized to NIST-610

364 but do not apply a secondary correction for matrix-dependent fractionation.

365 For the biotites analysed in our study, the fully propagated 95% confidence interval uncertainties

366 ranges between 0.8 and 1.6% when calibrated to Mica-Mg and between 1.0% and 1.4% when

367 calibrated to NIST-610 and corrected to MDC (depending on the sample and analytical session;

368 Table 3), allowing for more detailed accuracy comparisons. Figure 4 illustrates that using NIST-

369 610 and MDC as calibration reference materials produces the most accurate results, compared to

370 the expected references dates. For the biotite results, the obtained Rb–Sr dates are within 0.5%

371 accuracy compared to the expected ages. The K-feldspar dates are accurate within 1%, except for

372 session 2, where accuracy is within 1.5%. When the same data is calibrated against Mica-Mg

373 (either using NIST-610 as the PRM and Mica-Mg as MCRM, or directly using Mica-Mg as the

374 PRM), the results are significantly offset from their expected ages. For the biotite results calibrated

375 to Mica-Mg, accuracy is within 2% for sessions 2 and 3 and there is 5% age off-set in session 1.

376 For the K-felspars, the age offset is up to 2.5% in sessions 2 and 3 and 6% in session 1. While the

377 age offsets in sessions 2 and 3 might be regarded as `acceptable`, given the obtained precision, the

378 more significant inaccuracy in session 1 renders Mica-Mg to be less desirable as a PRM.

379 The difference in accuracy between session 1 and sessions 2 and 3 can be explained by the

380 difference in measured dates for the MDC and Mica-Mg reference materials, normalised to NIST-

381 610. For sessions 2 and 3, MDC and Mica-Mg produced similar isochron dates (2.3 and 1.9%

382 difference respectively) (Table 3; Fig. 6). For session 1, however, MDC gives a significantly

383 different age (494 ± 4 Ma) compared to Mica-Mg (469 ± 4 Ma). These differences in accuracy (ca.

384 5 % in session 1 and ca. 2 % in sessions 2 and 3) are in line with the observed age off-sets between

385 the measured dates and reference dates for the biotite and K-feldspar samples, calibrated to Mica-

386 Mg.

387

388 **5.2.3. Long-term comparison between MDC and Mica-Mg as secondary calibration**

389 **standards**

390 Given that the accuracy of the Rb–Sr method appears to be significantly dependent on the applied

391 calibration reference materials, and that the measured Rb–Sr dates of these calibration standards

392 fluctuate significantly between analytical sessions when compared to NIST-610, the long-term

393 behaviour of the MDC and Mica-Mg reference materials needs to be evaluated. Figure 7 presents

394 2.5 years of measured Rb–Sr dates for MDC and Mica-Mg, both calibrated to NIST-610 as the

395 PRM. All data in this plot have been processed identically. The Rb–Sr dates for Mica-Mg are

396 generally more consistent, ranging between ca. 462 and 479 Ma, with a standard deviation of 4.5

397 Ma, while the MDC dates show more variation, ranging between ca. 465 and 494 Ma, with a

398 standard deviation of 7.7 Ma. In all but two sessions, MDC produces an older Rb–Sr date compared

399 to Mica-Mg. The analytical sessions discussed above are highlighted in Figure F and encompass

400 the maximum variability in measured Rb–Sr dates for MDC. With the premise that calibration to

401 NIST-610 and MDC produces accurate Rb–Sr dates (as discussed in section 5.2.2), the difference

402 between the measured MDC and Mica-Mg dates (Fig. 6, 7) can be regarded as an estimate of the

403 degree of inaccuracy when data is calibrated to Mica-Mg. While some sessions reveal very little

404 off-set between both standards, using Mica-Mg as calibration standard can lead to up to 5%

405 inaccuracy in Rb–Sr dates. The cause of the observed variability is currently unknown, however,

406 in the second-to-last session with a significantly older Mica-Mg date compared to MDC, the

407 analysed samples might have received a lower effective laser fluence compared to other sessions

408 as the glass between the laser beam and samples was not cleaned prior to analysis. The lower

409 fluence could change the effective matrix bias between NIST-610, Mica-Mg and MDC, however,

410 calibration of biotite against MDC produces accurate results as demonstrated in section 5.2.2. In

411 contrast, although Mica-Mg produces more consistent Rb–Sr dates between analytical sessions,

412 these dates are unreliable given the variable and unsystematic degree of inaccuracy between

413 sessions.

414

415 **6. Conclusions**

416 Based on our observations, the use of Mica-Mg as calibration reference material is not

417 recommended, for the following reasons:

418 (1) The down-hole fractionation (DHF) trend for Mica-Mg is not comparable with the DHF

419 trends of natural bitote, phlogopite and K-feldspar (Fig. 1). Using Mica-Mg to correct DHF

420 would exacerbate instead of reduce DHF in those minerals;

421   (2) Given the relatively poor reproducibility of $^{87}Rb/^{87}Sr$ ratios and significant uncertainty on

422   individual $^{87}Sr/^{86}Sr$ measurements (Fig. 2), Mica-Mg as PRM or MCRM introduces excess

423   uncertainty that can be avoided using a more consistent PRM such as NIST-610;

424   (3) We demonstrated that calibrating to Mica-Mg may lead to up to 5% inaccuracy in Rb–Sr

425   age (Fig. 4, 6, 7) and that the degree of inaccuracy is unsystematically session-dependant.

426 We suggest a different approach, involving (1) calibration of the $^{87}Rb/^{87}Sr$ and $^{87}Sr/^{86}Sr$ ratios to a

427 primary reference material with high Rb and Sr concentrations and homogenous isotopic ratios

428 such as NIST-610 glass, including DHF correction of the Rb/Sr ratios, followed by (2) a correction

429 of the $^{87}Rb/^{87}Sr$ ratio to a natural mineral MCRM with a similar DHF trend as the samples to be

430 analysed. In our observations with a 67µm spot-size, there are no significant differences in matrix

431 effects comparing biotite, phlogopite and K-feldspar, suggesting that any of these natural minerals

432 as MCRM can produce accurate dates for K-rich minerals. We have used MDC phlogopite as

433 MCRM and demonstrate accurate Rb–Sr dates for a range of biotites and K-feldspars with well-

434 established age constraints. For the biotie dates, the fully propagated uncertainties for the analysed

435 biotites are <1.5 %, allowing accuracy verifications at high analytical precision. The K-feldspar

436 dates have relative high uncertainties (ca. 5-10%) and, therefore, the accuracy of the calibration

437 cannot robustly be tested. However, absolute values agree with biotite dates and for a given sample,

438 biotite and K-feldspar analyses statistically constitute a single isochron.

439 Finally, while this two-step calibration protocol is currently recommended due to current

440 constraints with data processing software, new developments involving calibrating to isochronous

441 reference materials might become the desired approach in the future.

442

443 **Data availability**

444 The Rb–Sr dataset used in this manuscript is freely available on figshare at
445 https://doi.org/10.25909/23996484.
446
447
448 **Acknowledgements**

449 This paper was supported by research grant FT210100906 and DP220103037 from the Australian
450 Research Council (ARC).

451
452
453 **Author contributions**

454 SG: Conceptualization, investigation, writing – original draft, methodology, funding acquisition,
455 visualisation, formal analysis

456 SEG: Conceptualization, investigation, writing – review and editing, methodology

457 MH: Conceptualization, investigation, writing - review and editing, resources

458 JCL: Conceptualization, investigation, writing - review and editing, formal analysis

459

460 **Competing interests**

461 The authors declare that they have no conflict of interest.

462

463 **Ethical statement**

464 This manuscript is an original work that is not submitted or published elsewhere.

465

	React. gas (ml.min^{-1})	Laser wavel. (nm)	Fluence (J.cm^{-2})	Rep. rate (Hz)	Spot (µm)	Rb-Sr calibration	Sr-Sr calibration	DHF	Err. corr.
Zack and Hogmalm 2016	O$_2$ (0.25)	213	7	10	80	Pl: NIST-610; Ksp: BCR-2G; Bt: La Posta	NIST-610	No	No
Hogmalm et al. 2017	O$_2$ (0.25) N$_2$O (0.16) SF$_6$ (0.04)	213	O$_2$: 7 N$_2$O: 6-8 SF$_6$: 6-8	10 4-5 10	80 50 50	Mica-Mg	NIST-610	No	No
Tillberg et al. 2020	N$_2$O (?)	213	?	?	50	BCR-2G (Sec: Mica-Mg/La Posta)	NIST-610	No	Yes
Rösel and Zack 2022	N$_2$O (0.18-0.20)	213	5-7	10	50-60	Mica-Mg (sec: NIST-610 / BCR-2G)	Mica-Mg	No	No
Gorojovsky and Alard 2020	N$_2$O (0.25)	193 and 213	7.8	5	85	Mica-Mg	Mica-Mg, NIST-610, BHVO-2G	No	No?
Larson et al 2023	N$_2$O (0.37)	193	4	10	50	Mica-Mg (Sec: Mica-Fe)	NIST-610	Yes?	Yes
Laureijs et al. 2021	CH$_3$F (10%)	213	6	10	50	ATHO-G, T1-G, StHs6/80-G	NIST-612	No	Yes
Li et al. 2020	N$_2$O (0.35)	193	3.5	5	74	Mica-Mg Sec: MDC	Mica-Mg	No	No
Liebmann et al. 2022	N$_2$O (?)	193	2.5	5	64	NIST-610 + Mica-Mg Sec: CK001 bt	NIST-610	No	Yes
Olierook et al. 2020	N$_2$O (0.25)	193	2.5	5	64-87	NIST-610 + Mica-Mg Sec: CK001 bt	NIST-610	No	No
Redaa et al. 2021	N$_2$O (0.37)	193	3.5	5	74	Mica-Mg Sec: MDC	Mica-Mg	monitored	No
Sengun et al. 2019	N$_2$O (?)	213	5.7	10	50	Mica-Mg	NIST-610	No	No
Tilberg et al. 2021	N$_2$O (?)	213	?	?	50	Mica-Mg / NIST 610	NIST-610	No	Yes
Wang et al. 2022	N$_2$O (0.25)	193	7	5	85	Mica-Mg	NIST-610, BHVO-2G, BCR-2G	monitored	No
Kirkland et al. 2023	N$_2$O (0.25)	193	2	5	64	Mica-Mg Sec: CK001 bt	NIST-610	No	No

467   **Table 1:** Summary of published analytical conditions and protocols for LA-ICP-MS/MS Rb–Sr

468   dating. Rep. rate = laser repetition rate; Sec = secondary reference material; Bt = biotite; ksp = K-

469   feldspar; Pl = plagioclase; Err. Corr. = error correlation calculated (in most cases based on

470   calculated uncertainties after data-reduction rather than during data-reduction); In case of method

471   development work - `best conditions` are quoted.

472

Analytical conditions	
Plasma Settings	
RF power	1350 W
Sample Depth	5.0 mm
Ar carrier gas	0.89 L/min
He carrier gas	0.38 L/min
N_2 addition	4 mL/min
Lens Parameters	
Extract 1	1.5 V
Extract 2	-80 V
Omega Bias	-85 V
Omega Lens	5.0 V
Q1 entrance	-10 V
Q1 exit	-2.0 V
Cell focus	-2.0 V
Cell Entrance	-90 V
Cell Exit	-120 V
Deflect	10 V
Plate Bias	-80 V
Q1 bias	-2.0 V
Q1 Prefilter Bias	-10.0 V
Q1 Postfilter Bias	-10.0 V
N_2O gas flow	0.37 mL/min
Octopole bias	-6.0 V
Axial Acceleration	2.0 V
Octopole RF	180 V
Energy Discrimination	-7.0 V
Analysis Parameters	
Laser Wavelength	193 nm
Laser fluence	3.5 J/m2
Sample laser diameter	67 μm
Laser repetition rate	5 Hz
Background	30 s
Analysis time	40 s
Isotopes measured & dwell times (ms)	^{23}Na (2), ^{24}Mg (2), ^{27}Al (2), $^{29+16}$Si (2), $^{31+16}$P (2), ^{39}K (2), $^{43+16}$Ca (2), ^{55}Mn (2), $^{56+16}$Fe (2), ^{85}Rb (10), $^{86+16}$Sr (50), $^{87+16}$Sr (50), $^{88+16}$Sr (50), $^{89+16}$Y (5), $^{90+32}$Zr (5), $^{93+32}$Nb (5), all $^{x+16}$REE (5), $^{232+15}$Th (5), $^{238+16}$U (5)

473
474

475 **Table 2:** Analytical conditions for the three LA-ICP-MS/MS sessions in this paper.

Sample (exp. age)	S	n	(A) NIST-610 + MDC Age (± 2σ) [Ma]	MSWD	(B) NIST610 + Mica-Mg Age (± 2σ) [Ma]	MSWD	(C) Mica-Mg & NIST-610 Age (± 2σ) [Ma]	MSWD	(D) Mica-Mg Age (± 2σ) [Ma]	MSWD
Ent Crk Bt	1	24	310.7 ± 1.5/2.5/3.1	1.1	327.8 ± 1.7/2.7/3.2	0.96	327.6 ± 3.3/3.9	0.27	328.8 ± 3.4/4.0	0.25
(312.1 ± 1.8[1])	3	20	311.6 ± 3.1/3.8/4.5	2.5	317.6 ± 3.2/3.8/4.6	2.4	316.1 ± 3.2/3.8	0.85	316.2 ± 3.2/3.8	0.84
Bund1b Bt	2	44	287.1 ± 1.6/2.4/3.4	1.6	280.3 ± 1.5/2.4/3.2	1.7	280.1 ± 1.6/2.4	0.97	280.2 ± 1.6/2.4	0.82
(286.2 ± 2.2[2])	3	22	284.7 ± 2.4/3.0/3.8	1.0	290.1 ± 2.5/3.1/3.8	1.1	288.4 ± 4.1/4.5	0.7	288.2 ± 4.3/4.7	0.28
Bund1b Ksp	2	57	290 ± 14/14/14	0.87	284 ± 14/14/14	0.88	284 ± 14/14	0.84	280 ± 23/23	0.3
(286.2 ± 2.2[2])	3	53	287 ± 15/15/15	0.88	292 ± 15/15/15	0.88	290 ± 15/16	0.86	283.4 ± 38/38	0.19
Bund6a Bt	2	38	287.7 ± 1.3/2.3/3.4	1.4	280.9 ± 1.3/2.2/3.1	1.5	279.5 ± 1.5/2.3	0.71	279.5 ± 1.5/2.3	0.7
(286.2 ± 2.2[2])	3	22	285.7 ± 1.9/2.6/3.4	0.74	291.2 ± 1.9/2.7/3.6	0.72	288.7 ± 3.5/4.0	0.54	288.8 ± 3.6/4.0	0.34
Bund6a Ksp	2	45	290 ± 37/37/37	0.69	283 ± 36/36/36	0.69	281 ± 36/36	0.68	283 ± 75/75	0.16
(286.2 ± 2.2[2])	3	40	288 ± 37/37/37	0.65	293 ± 38/38/38	0.65	294 ± 39/39	0.65	296 ± 93/93	0.11
Taratap Bt	2	30	499.4 ± 1.8/3.6/5.6	1.2	487.7 ± 1.7/3.5/5.2	1.2	489.6 ± 2.8/4.2	0.67	489.6 ± 2.8/4.2	0.63
(497.1 ± 0.6[3])	3	16	495.7 ± 2.5/4.0/5.5	1.2	505.1 ± 2.6/4.1/5.8	1.2	504.0 ± 5.4/6.3	0.51	504.0 ± 5.5/6.3	0.52
Taratap Ksp	1	54	500 ± 30/30/30	0.53	527 ± 31/31/31	0.53	527 ± 32/32	0.50	539 ± 58/58	0.14
(497.1 ± 0.6[3])	2	20	501 ± 50/50/50	0.58	490 ± 49/49/49	0.58	492 ± 50/50	0.56	494 ± 106/106	0.12
	3	18	495 ± 35/35/35	0.95	504 ± 36/36/36	0.95	490 ± 39/39	1.1	511 ± 63	0.3

476

477

MCRM	S	n	NIST-610 as PRM Age (± 2σ) [Ma]	MSWD
MDC	1	34	494.4 ± 3.0	1.4
	2	21	464.5 ± 4.0	1.3
	3	30	470.6 ± 3.6	1.1
Mica-Mg	1	35	468.6 ± 2.5	2.8
	2	21	475.7 ± 3.7	3.5
	3	20	461.8 ± 3.7	2.7

478

479

480 **Table 3:** Summary table of Rb–Sr dates obtained in this study. S = session number, n = number of analysed grains, exp. age = expected

481 reference age (see below). All uncertainties are 95% confidence intervals and are reported as (1) excluding external uncertainty (on the

482 decay constant) / (2) including external uncertainties / (3) with propagated uncertainty from the correction standard (for methods (A)

483 and (B) only). (A) NIST-610 as PRM and MDC as MCRM to calibrate Rb/Sr ratios; (B) NIST-610 as PRM, Mica-Mg as MCRM to

484 calibrate Rb/Sr ratios; (C) Rb/Sr ratios calibrated to Mica-Mg as PRM and Sr/Sr ratios calibrated to NIST-610 as PRM; (D) Mica-MG

485 as PRM for both Rb/Sr and Sr/Sr ratios. [1] Rb-Sr TIMS age from Mortimer et al. (1987), recalculated with Villa et al. (2015) decay

486 constant in IsoplotR (Vermeesch, 2018). The reported uncertainty is 95% confidence interval but does not take overdispersion into

487 account. [2] Zircon U-Pb age for the Banalasta Adamellite in the Bundarra Suite, from Black (2007). [3] Zircon U-Pb TIMS age for the

488 Taratap Granodiorite, reported in Glorie et al. (2023).

489

490 **Figure Captions**

491
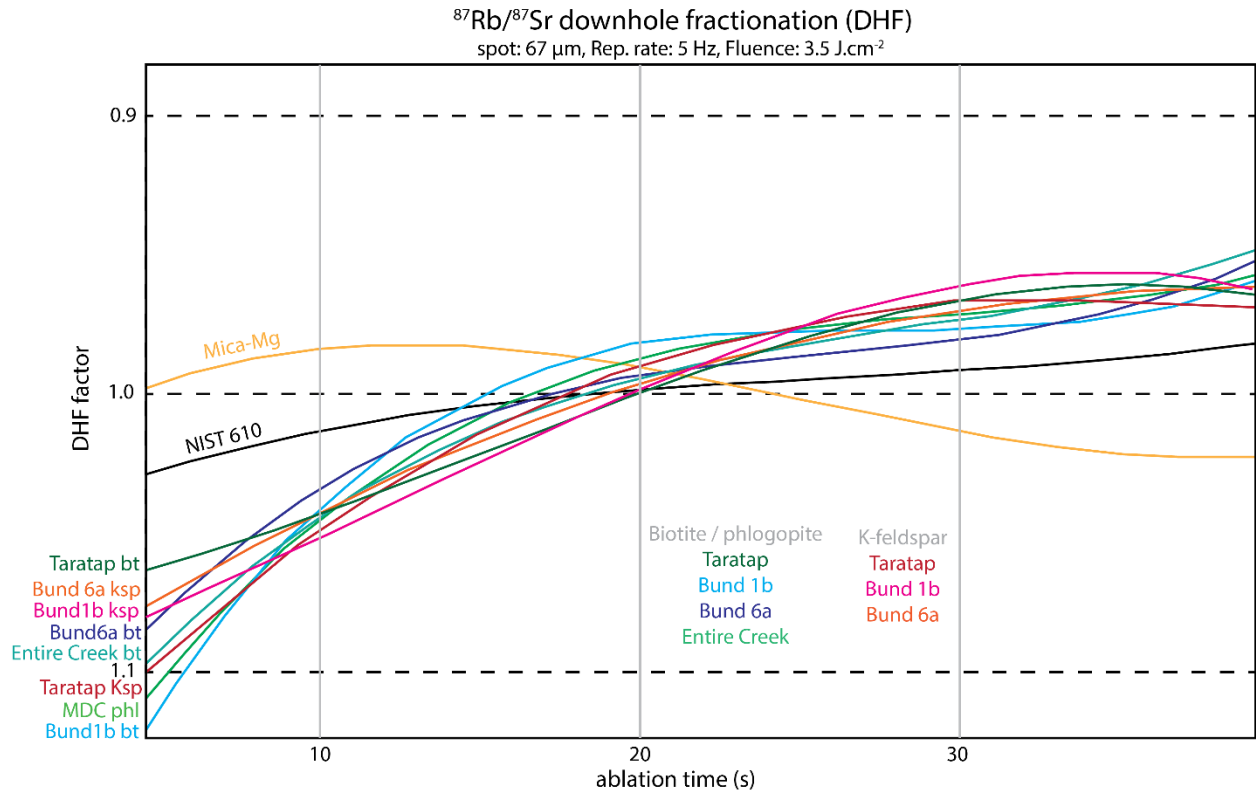
492

493 **Figure 1:** [87]Rb/[87]Sr downhole fractionation profiles for the analysed reference materials Mica-Mg

494 (yellow line) and NIST-610 (black line), the biotite / phlogopite (green-blue lines) and K-felspar

495 (red-pink lines) samples in analytical session 3, calculated in LADR (Norris and Danyushevsky,

496 2018). The DHF factor is calculated relative to the average ratio of the ablation signal (i.e. DHF

497 factor of 1 = average [87]Rb/[87]Sr ratio of the downhole signal).

498

499
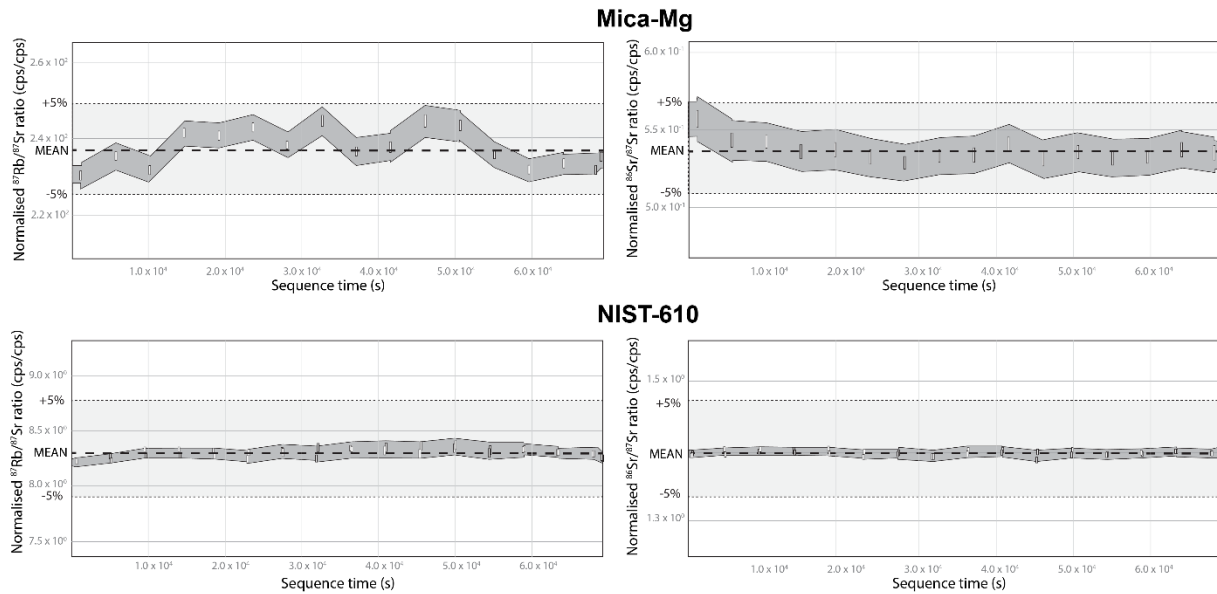
Figure 2: Variability of the $^{87}Rb/^{87}Sr$ and $^{86}Sr/^{87}Sr$ ratios for the analysed reference materials NIST-610 and Mica-Mg over the total duration of analytical session 3 ==(prior to drift correction)==. All plots are scaled equally to ± 5% variation of the mean to aid visual comparisons. The vertical bars are ±1 standard deviation. The gray envelopes models ±2 standard deviation (note that for NIST-610 each standard was measured twice at each standard bracket).

505
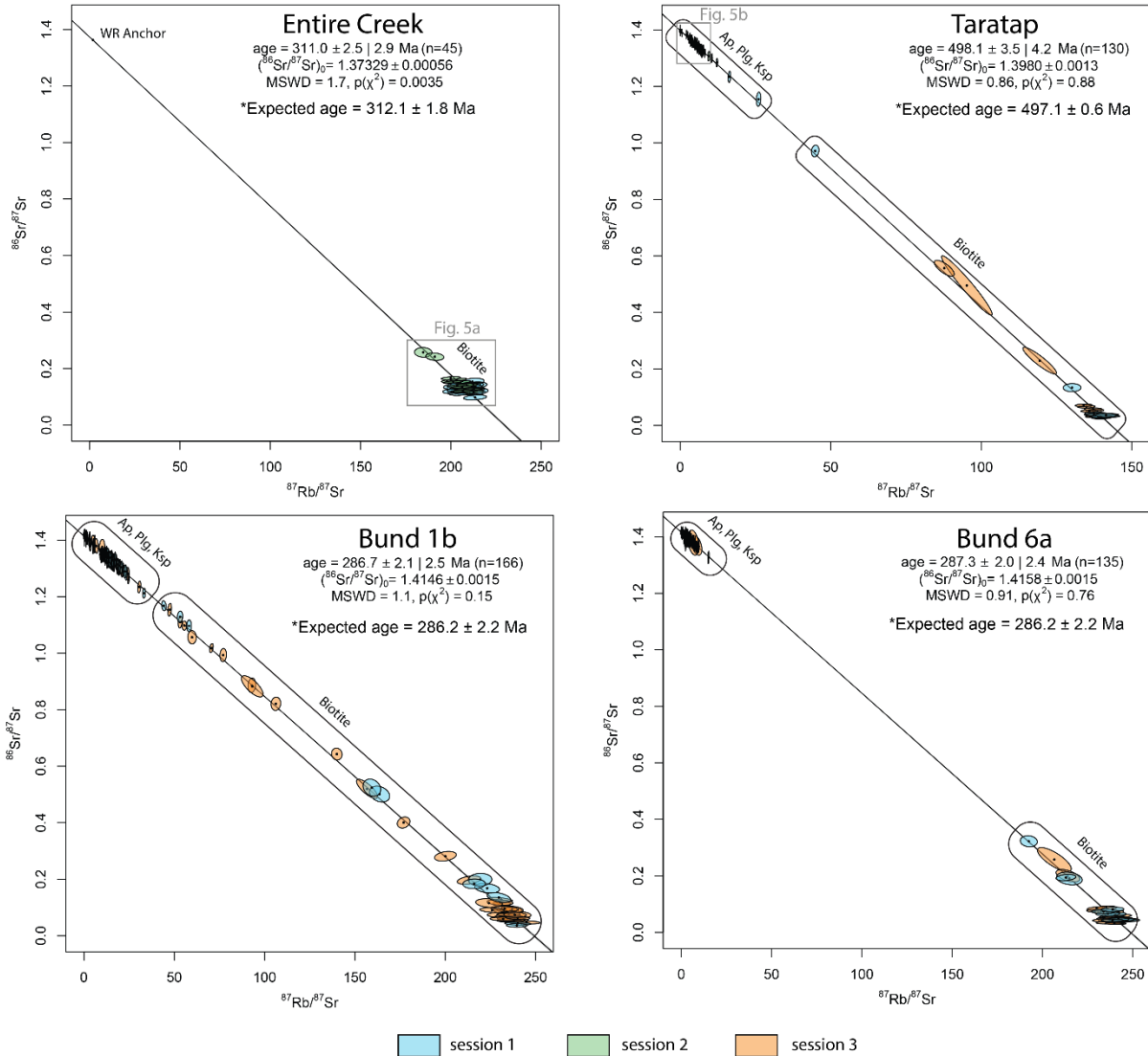
Figure 3: Pooled multi-mineral Rb–Sr isochron dates for the Entire Creek, Taratap and the two Bundarra samples (Bund 1b and Bund 6a). The data was calibrated against NIST-610 as PRM and MDC as MCRM (see text for details). The colour-code refers to the analytical session in which the data was obtained. Biotite analyses plot towards the radiogenic lower-intercept of the inverse isochrons, while feldspar and apatite anchor Rb/Sr ratios plot towards the low-radiogenic end of the isochron regression. All plots were calculated in IsoplotR (Vermeesch, 2018), reporting 95% confidence interval uncertainties (including the uncertainty on the decay-constant) with and without propagated uncertainty from the MDC MCRM. Expected ages are the recalculated Rb–Sr

515   age from Mortimer et al. (1987) with the Villa et al. (2015) decay constant for the Entire Creek

516   sample; the zircon U-Pb ID-TIMS age reported in Glorie et al. (2023) for the Taratap sample, and

517   the Zircon SHRIMP U-Pb age from Black (2007) for the Bundarra samples (see text for further

518   details).

519
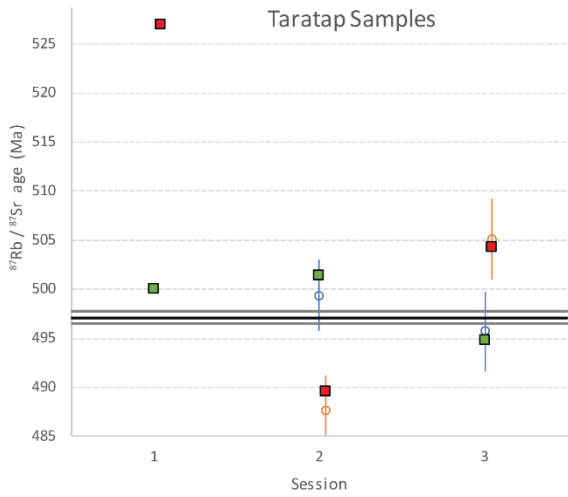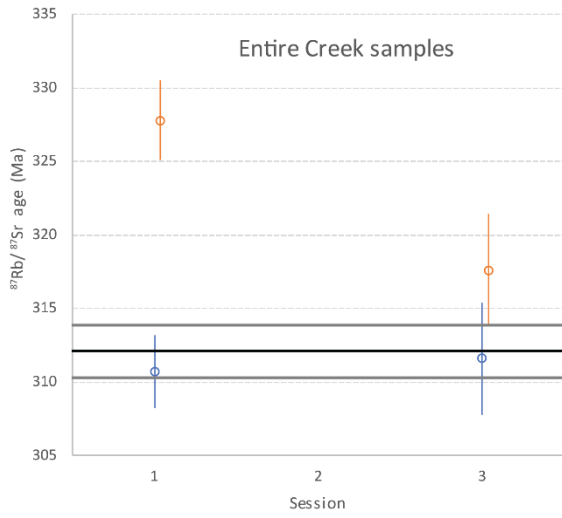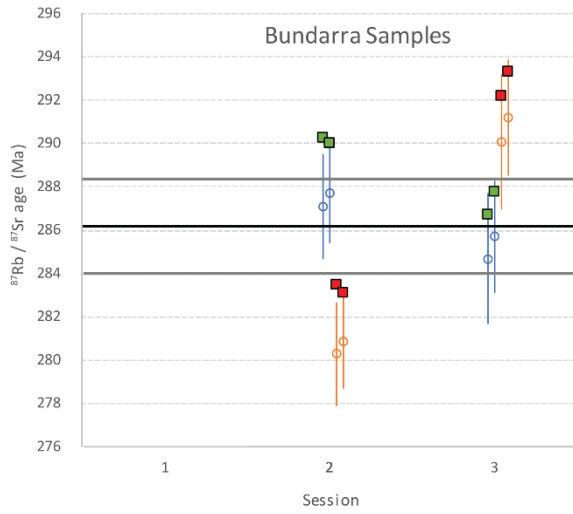
521 **Figure 4:** Comparisons of Rb–Sr dates over three analytical sessions, calibrated to either MDC or

522 Mica-Mg as MCRM, with respect to the expected ages for each sample (black line with gray 2SE

523 uncertainty bars). In all cases, NIST-610 was used as PRM. Biotite data are plotted as open circles

524 (blue = calibrated to MDC as MCRM, orange = calibrated to Mica-Mg as MCRM). K-feldspar

525 data are plotted as filled squares (green = calibrated to MDC as MCRM, red = calibrated to Mica-

526 Mg as MCRM).

527
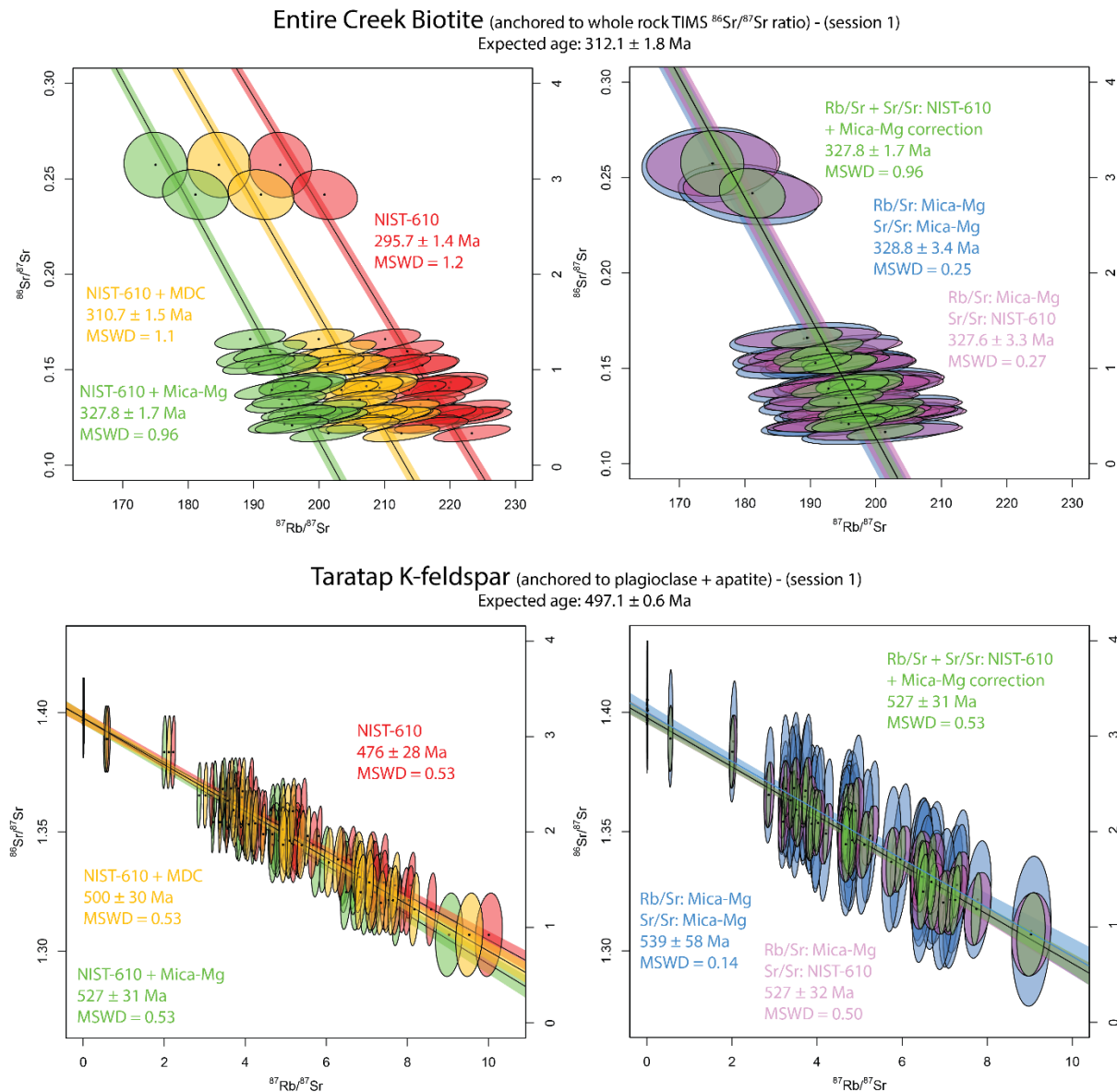
528

529   **Figure 5:** Comparisons of isochron dates obtained using the 4 different calibration protocols using

530   the session 1 biotite Rb–Sr data from the Entire Creek sample and K-feldspar Rb–Sr data from the

531   Taratap sample. Data plotted in red = NIST-610 as PRM without correction for matrix-induced

532   fractionation. Data plotted in green = NIST-610 as PRM with Mica-Mg as MCRM. Data plotted

533   in yellow = NIST-610 as PRM with MDC as MCRM. Data plotted in purple = NIST-610 as PRM

534   for Sr/Sr ratios and Mica-Mg as PRM for Rb/Sr ratios. Data plotted in blue = both Rb/Sr and Sr/Sr

535   ratios calibrated to Mica-Mg as PRM. The biotite data are highly radiogenic and show significant

536   age differences depending on the used MCRM. The K-feldspar data are low radiogenic, resulting

537   in larger and overlapping uncertainties (refer to Figure 3 for full isochron plots). Using NIST-610

538   as PRM produces the smallest uncertainties on individual data-points.

539
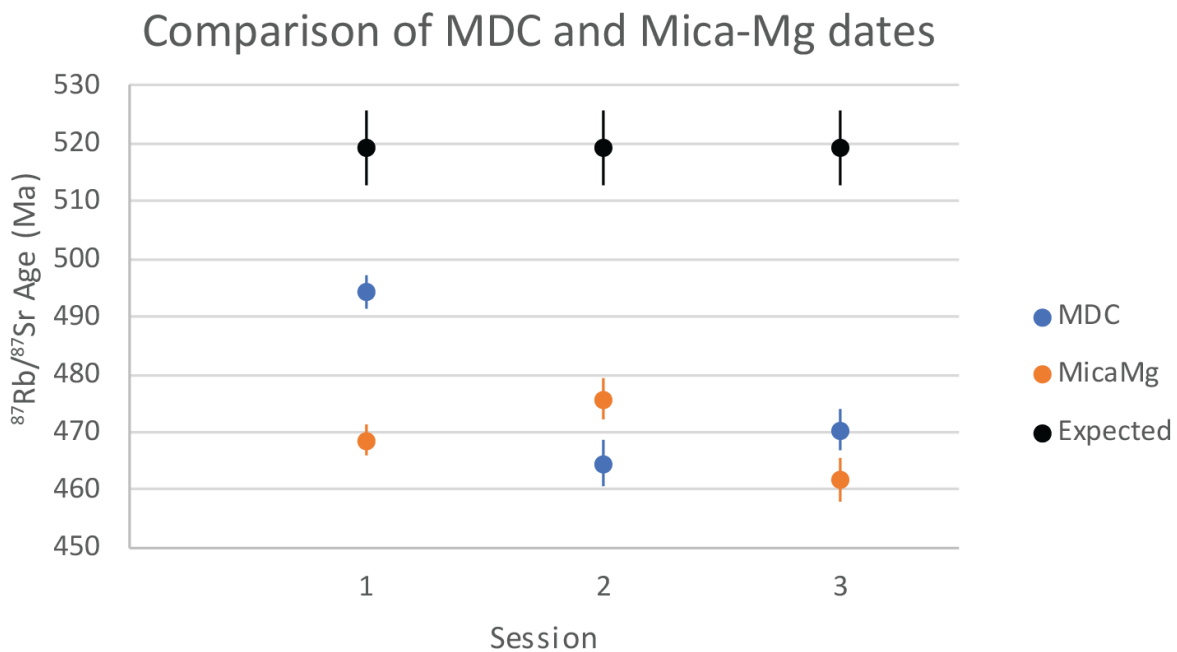
540

541 **Figure 6:** Rb–Sr dates for MDC and Mica-Mg calibrated to NIST-610 over the three analytical

542 sessions used in this paper. The off-set of the Rb–Sr age with respect to the reference age is used

543 to calculate the correction factor on the Rb/Sr ratios. Uncertainties are 2SE.

544

545

546 **Figure 7:** Long-term (2.5 years) Rb–Sr age data for Mica-Mg and MDC for the lab (Adelaide

547 Microscopy). All uncertainties are 2SE. The top plot shows absolute dates and the bottom plot

548 shows the percentage difference between the MDC and Mica-Mg dates. All data were processed

549   in the same way using NIST-610 as PRM. The three analytical sessions previously discussed are

550   highlighted by black rims and capture the most extreme differences obtained in our lab to date.

551   Given that MDC as ==MC==RM produces consistently accurate data, the plot indicates that Mica-Mg

552   as PRM can lead to up to 5% inaccuracy in Rb–Sr age calculations.

553

References

555 Balcaen, L., Bolea-Fernandez, E., Resano, M., Vanhaecke, F., 2015. Inductively coupled plasma – Tandem
556   mass spectrometry (ICP-MS/MS): A powerful and universal tool for the interference-free
557   determination of (ultra)trace elements – A tutorial review. Analytica Chimica Acta, 894: 7-19.
558 Black, L., 2007. SHRIMP U–Pb zircon ages obtained during 2006/07 for NSW Geological Survey projects.
559 Burtt, A.C., Abbot, P.J., 1998. The Taratap Granodioritite, South-East South Australia. MESA Journal, 10:
560   35-39.
561 Flood, R.H., Shaw, S.E., 1975. A cordierite-bearing granite suite from the New England Batholith, N.S.W.,
562   Australia. Contributions to Mineralogy and Petrology, 52(3): 157-164.
563 Flood, R.H., Shaw, S.E., 1977. Two "S-type" granite suites with low initial 87Sr/86Sr ratios from the New
564   England Batholith, Australia. Contributions to Mineralogy and Petrology, 61(2): 163-173.
565 Glorie, S. et al., 2023. Robust laser ablation Lu-Hf dating of apatite: an empirical evaluation. Geological
566   Society of London Special Publication, In press.
567 Gorojovsky, L., Alard, O., 2020. Optimisation of laser and mass spectrometer parameters for thein
568   situanalysis of Rb/Sr ratios by LA-ICP-MS/MS. JOURNAL OF ANALYTICAL ATOMIC SPECTROMETRY,
569   35(10): 2322-2336.
570 Hogmalm, K.J., Zack, T., Karlsson, A.K.O., Sjoqvist, A.S.L., Garbe-Schonberg, D., 2017. In situ Rb-Sr and K-
571   Ca dating by LA-ICP-MS/MS: an evaluation of N2O and SF6 as reaction gases. Journal of Analytical
572   Atomic Spectrometry, 32(2): 305-313.
573 Jackson, S.E., Günther, D., 2003. The nature and sources of laser induced isotopic fractionation in laser
574   ablation-multicollector-inductively coupled plasma-mass spectrometry. Journal of Analytical
575   Atomic Spectrometry, 18(3): 205-212.
576 Jegal, Y. et al., 2022. Characterisation of Reference Materials for In Situ Rb-Sr Dating by LA-ICP-MS/MS.
577   Geostandards and Geoanalytical Research, 46(4): 645-671.
578 Jeon, H., Williams, I.S., Chappell, B.W., 2012. Magma to mud to magma: Rapid crustal recycling by Permian
579   granite magmatism near the eastern Gondwana margin. Earth and Planetary Science Letters, 319-
580   320: 104-117.
581 Kirkland, C.L. et al., 2023. Dating mylonitic overprinting of ancient rocks. Communications Earth &
582   Environment, 4(1): 47.
583 Košler, J. et al., 2005. Chemical and phase composition of particles produced by laser ablation of silicate
584   glass and zircon—implications for elemental fractionation during ICP-MS analysis. Journal of
585   Analytical Atomic Spectrometry, 20(5): 402-409.
586 Larson, K.P., Button, M., Shrestha, S., Camacho, A., 2023. A comparison of 87Rb/87Sr and 40Ar/39Ar
587   dates: Evaluating the problem of excess 40Ar in Himalayan mica. Earth and Planetary Science
588   Letters, 609: 118058.

589 Laureijs, C.T., Coogan, L.A., Spence, J., 2021. In-situ Rb-Sr dating of celadonite from altered upper oceanic
590   crust using laser ablation ICP-MS/MS. Chemical Geology, 579.

591 Li, S.-S. et al., 2020. Coupled U-Pb and Rb-Sr laser ablation geochronology trace Archean to Proterozoic
592   crustal evolution in the Dharwar Craton, India. Precambrian Research, 343: 105709.

593 Li, Y., Vermeesch, P., 2021. Short communication: Inverse isochron regression for Re–Os, K–Ca and other
594   chronometers. Geochronology, 3(2): 415-420.

595 Liebmann, J., Kirkland, C.L., Kelsey, D.E., Korhonen, F.J., Rankenburg, K., 2022. Lithological fabric as a proxy
596   for Rb-Sr isotopic complexity. Chemical Geology, 608.

597 Longerich, H.P., Günther, D., Jackson, S.E., 1996. Elemental fractionation in laser ablation inductively
598   coupled plasma mass spectrometry. Fresenius' Journal of Analytical Chemistry, 355(5): 538-542.

599 Moens, L.J., Vanhaecke, F.F., Bandura, D.R., Baranov, V.I., Tanner, S.D., 2001. Elimination of isobaric
600   interferences in ICP-MS, using ion–molecule reaction chemistry: Rb/Sr age determination of
601   magmatic rocks, a case study. Journal of Analytical Atomic Spectrometry, 16(9): 991-994.

602 Mortimer, G.E., Cooper, J.A., James, P.R., 1987. U□Pb and Rb□Sr geochronology and geological
603   evolution of the Harts Range ruby mine area of the Arunta Inlier, central Australia. Lithos, 20(6):
604   445-467.

605 Norris, A., Danyushevsky, L., 2018. Towards Estimating the Complete Uncertainty Budget of Quantified
606   Results Measured By LA-ICP-MS. Goldschmidt, Boston, USA (2018).

607 Olierook, H.K.H. et al., 2020. Resolving multiple geological events using in situ Rb–Sr geochronology:
608   implications for metallogenesis at Tropicana, Western Australia. Geochronology, 2(2): 283-303.

609 Phillips, G., Landenberger, B., Belousova, E.A., 2011. Building the New England Batholith, eastern
610   Australia—Linking granite petrogenesis with geodynamic setting using Hf isotopes in zircon.
611   Lithos, 122(1): 1-12.

612 Redaa, A. et al., 2023. Testing Nano-Powder and Fused-Glass Mineral Reference Materials for In Situ Rb-
613   Sr Dating of Glauconite, Phlogopite, Biotite and Feldspar via LA-ICP-MS/MS. Geostandards and
614   Geoanalytical Research, 47(1): 23-48.

615 Redaa, A. et al., 2021. Assessment of elemental fractionation and matrix effects during in situ Rb-Sr dating
616   of phlogopite by LA-ICP-MS/MS: implications for the accuracy and precision of mineral ages.
617   Journal of Analytical Atomic Spectrometry, 36(2): 322-344.

618 Roberts, N.M.W. et al., 2017. A calcite reference material for LA-ICP-MS U-Pb geochronology.
619   Geochemistry, Geophysics, Geosystems, 18(7): 2807-2814.

620 Rosel, D., Zack, T., 2022. LA-ICP-MS/MS Single-Spot Rb-Sr Dating. Geostandards and Geoanalytical
621   Research, 46(2): 143-168.

622 Rosenbaum, G., Li, P., Rubatto, D., 2012. The contorted New England Orogen (eastern Australia): New
623   evidence from U-Pb geochronology of early Permian granitoids. Tectonics, 31(1).

624 Sengun, F., Erlandsson, V.B., Hogmalm, J., Zack, T., 2019. In situ Rb-Sr dating of K-bearing minerals from
625   the orogenic Akcaabat gold deposit in the Menderes Massif, Western Anatolia, Turkey. JOURNAL
626   OF ASIAN EARTH SCIENCES, 185.

627 Shaw, S.E., Flood, R.H., 1981. The New England Batholith, eastern Australia: Geochemical variations in
628   time and space. Journal of Geophysical Research: Solid Earth, 86(B11): 10530-10544.

629 Simpson, A. et al., 2022. In situ Lu–Hf geochronology of calcite. Geochronology, 4(1): 353-372.

630 Tillberg, M. et al., 2021. Reconstructing craton-scale tectonic events via in situ Rb-Sr geochronology of
631   poly-phased vein mineralization. Terra Nova, 33(5): 502-510.

632 Tillberg, M. et al., 2020. In situ Rb-Sr dating of slickenfibres in deep crystalline basement faults. Scientific
633   Reports, 10(1).

634 Vermeesch, P., 2018. IsoplotR: A free and open toolbox for geochronology. Geoscience Frontiers, 9(5):
635   1479-1493.

636 Villa, I.M., De Bièvre, P., Holden, N.E., Renne, P.R., 2015. IUPAC-IUGS recommendation on the half life of
637   87Rb. Geochimica et Cosmochimica Acta, 164: 382-385.
638 Wang, C.Y. et al., 2022. Advances in in-situ Rb-Sr dating using LA-ICP-MS/MS: applications to igneous rocks
639   of all ages and to the identification of unrecognized metamorphic events. Chemical Geology, 610.
640 Woodhead, J.D., Hergt, J.M., 2001. Strontium, Neodymium and Lead Isotope Analyses of NIST Glass
641   Certified Reference Materials: SRM 610, 612, 614. Geostandards Newsletter, 25(2-3): 261-266.
642 Zack, T., Hogmalm, K.J., 2016. Laser ablation Rb/Sr dating by online chemical separation of Rb and Sr in an
643   oxygen-filled reaction cell. Chemical Geology, 437: 120-133.